Atherosclerosis 275 (2018) 1–10

Contents lists available at ScienceDirect

Atherosclerosis

journal homepage: www.elsevier.com/locate/atherosclerosis

# Activatable fluorescence imaging of macrophages in atherosclerotic plaques using iron oxide nanoparticles conjugated with indocyanine green

Hiroyuki Ikeda [a, b, *], Akira Ishii [a], Kohei Sano [b, c, **], Hideo Chihara [a], Daisuke Arai [a], Yu Abekura [a], Hidehisa Nishi [a], Masahiro Ono [b], Hideo Saji [b], Susumu Miyamoto [a]

[a] Department of Neurosurgery, Kyoto University Graduate School of Medicine, Kyoto, Japan
[b] Department of Patho-Functional Bioanalysis, Graduate School of Pharmaceutical Sciences, Kyoto University, Kyoto, Japan
[c] Department of Biophysical Chemistry, Kobe Pharmaceutical University, Kobe, Japan

ARTICLE INFO

*Article history:*
Received 19 November 2017
Received in revised form
1 May 2018
Accepted 16 May 2018
Available online 18 May 2018

*Keywords:*
Macrophage
Atherosclerosis
Nanoparticles
Plaque
Fluorescent imaging

ABSTRACT

*Background and aims:* Macrophages are key factors in the formation of unstable atherosclerotic plaques, which may be identified through macrophage imaging. We tested whether activatable fluorescence probes of iron oxide nanoparticles (IONPs) conjugated with indocyanine green (ICG) (IONP-ICG), consisting of biocompatible reagents, can visualize macrophages present in atherosclerotic plaques.
*Methods:* IONP-based probes conjugated with different numbers of ICG molecules were synthesized. Six-week-old spontaneously hyperlipidemic (SHL) mice were fed either a Western or normal diet for 14 weeks, and were intravenously injected with IONP-ICG (55.8 mg Fe/kg). Aortas were harvested 48 h later, and aortas containing atherosclerotic plaques were imaged.
*Results:* Phantom imaging studies using IONP-ICG solution demonstrated that the addition of surfactants to IONP-ICG solutions yielded fluorescence activation. Incubation of macrophages with IONP-ICG led to internalization of IONP-ICG and near infrared fluorescence (NIRF) activation. In NIRF imaging studies, intense fluorescence signals were clearly visible primarily at the margins of atherosclerotic plaques, and relatively weak signals were evident inside the plaques, demonstrating the feasibility of detection of NIRF signals at atherosclerotic plaques. In the quantitative evaluation of NIRF, administration of a probe conjugated with more ICG molecules led to a significant increase in the NIRF signal, indicating that probes with greater numbers of ICG molecules are effective for sensitive NIRF detection. SHL mice given a low-cholesterol normal diet showed a significantly lower NIRF signal compared with mice given the Western diet. Histologically, NIRF signals in atherosclerotic plaques strongly correlated with the location of macrophages, suggesting the possibility of NIRF macrophage imaging using IONP-ICG.
*Conclusions:* Localization of macrophages in atherosclerotic plaques may be achieved using the activatable NIRF probe, IONP-ICG.



## 1. Introduction

Macrophages play important roles in atherosclerotic plaque formation [1,2] and are known to be involved in the destabilization of atherosclerotic plaques [3,4]. Detection of macrophage-rich regions in blood vessels may therefore lead to the identification of unstable atherosclerotic plaques. Recently, near-infrared fluorescence (NIRF) imaging, which can detect sensitively with relatively good tissue permeability and minimal effects from autofluorescence, has been attracting attention for the detection of unstable atherosclerotic plaques [5–7].

Indocyanine green (ICG), an NIRF molecule approved for clinical use by the Food and Drug Administration (FDA) in the United States, is highly biocompatible [8], and several imaging studies using ICG

* Corresponding author. Department of Neurosurgery, Kyoto University Graduate School of Medicine, 54 Kawahara-cho, Shogoin, Sakyo-ku, Kyoto, 606-8507, Japan.
** Corresponding author. Department of Biophysical Chemistry, Kobe Pharmaceutical University, 4-19-1 Motoyama Kitamachi, Higashinada-ku, Kobe, 658-8558, Japan.
*E-mail addresses:* rocky@kuhp.kyoto-u.ac.jp (H. Ikeda), ksano@kobepharma-u.ac.jp (K. Sano).

https://doi.org/10.1016/j.atherosclerosis.2018.05.028
0021-9150/

conjugated to various carrier molecules to detect tumor cells have been reported [9–13]. In the first place, ICG is the only NIRF imaging probe targeting inflamed atherosclerotic plaques that can be used clinically [14,15]. The circulating ICG binds rapidly to low-density and high-density lipoproteins in the blood, due to its lipophilic properties, and then the complexes of lipoproteins bound to ICG are taken up by macrophages of atherosclerotic plaques [14]. In this way, the uptake of ICG by macrophages is an indirect passage; but the direct uptake seems to be more effective for accurately visualizing macrophages. After injection, circulating ICG is rapidly taken up by liver and then released with an elimination half-life of 2–4 min [16], suggesting that almost all the injected ICG can't reach macrophages. For these reasons, imaging probes, which are directly taken up by macrophages and have a long circulating half-life are considered to be more effective than ICG. The fluorescent signals of ICG molecules can be quenched via a self-quenching mechanism in which interactions between ICG molecules occur when multiple fluorescent molecules are in close proximity [17]. Furthermore, the auto-quenching mechanism can contribute to fluorescent quenching of ICG where ICG molecules interact with carrier molecules [12,13]. Based on these mechanisms, the fluorescent signals of activatable ICG-labeled probes are active only when taken up by the target cells followed by lysosomal degradation, enabling the suppression of background signals from non-target tissues and more specific visualization of the target cells [18,19]. For these reasons, in comparison to other agents such as activatable NIRF probes and the Cy5.5/Cy7-labeled macrophage mannose receptors tracer, which can detect inflamed atherosclerotic plaques [5,20,21], activatable ICG-labeled probes with high background ratio are biocompatible NIRF imaging probes, and this allows their clinical application.

In contrast, iron oxide nanoparticles (IONPs), which are biocompatible and biodegradable molecules with low toxicity, have been used in a wide range of biomedical applications [22] and have been approved as an intravenous magnetic resonance (MR) contrast agent (Resovist®; Bayer Healthcare, Berlin, Germany) since 2001 in the European market [23]. IONPs are MR imaging probes that can locally accumulate at inflammatory sites where macrophages are present and can also change the magnetic field through nonspecific receptor-mediated endocytosis, especially scavenger receptors by macrophages. By exploiting these properties, the presence of macrophages in atherosclerotic plaques can be detected [7,24,25]. Therefore, we deduced that NIRF probes synthesized using the highly biocompatible fluorescent molecule ICG, and the carrier molecule IONP will be activatable fluorescent probes and may have the potential for clinical application to detect the macrophages associated with inflammation in atherosclerotic plaques.

Furthermore, since the *in vivo* kinetics of the carrier molecule can potentially be affected when conjugated with a large number of fluorescent molecules [9,11,26], we synthesized and compared probes with different numbers of ICG molecules per IONP molecule with regard to the *in vivo* biodistribution. The present study tested the hypothesis that IONPs conjugated with ICG as a biocompatible and activatable fluorescent probe would be capable of visualizing the macrophages present in atherosclerotic plaques.

## 2. Materials and methods

Details of the Materials and methods section are presented in the Supplementary Data.

### 2.1. Reagents

IONPs coated with dextran (nanomag®-D-spio; diameter, 20 nm; mean molecular weight, 3500 kDa, amino groups on particle surface) were purchased from Corefront Co. (Tokyo, Japan). ICG-EG4-Sulfo-OSu was purchased from Dojindo Molecular Technologies (Kumamoto, Japan). Methoxy polyethylene glycol (PEG) succinate N-hydroxysuccinimide (NHS) (PEG-NHS ester; molecular weight: 2 kDa, SUNBRIGHT ME-020CS) was purchased from NOF America Co. (White Plains, NY).

### 2.2. Preparation of IONPs conjugated with ICG

We synthesized IONPs conjugated with ICG probes (IONP-ICG; Supplemental Fig. 1). IONP-ICG synthesized at IONP:ICG molecular ratios of 1:5, 1:10, and 1:20 was denoted as IONP-ICG5, IONP-ICG10, and IONP-ICG20, respectively, according to the number of ICG molecules mixed with IONP.

### 2.3. Cell culture and phagocytotic activity of macrophage cells in vitro

NR8383 (rat alveolar macrophage cell line; ATCC CRL-2192) was purchased from the American Type Culture Collection (ATCC) center (Manassas, VA). Cells were incubated for 1, 8, 24, and 48 h followed by washing once with phosphate-buffered saline (PBS), and fluorescence microscopy was performed. Subsequently, iron staining was performed using a Berlin blue staining set (Wako Pure Chemical Industries, Osaka, Japan).

### 2.4. Animals

All animal experiments were performed in accordance with institutional guidelines and were approved by the Kyoto University Animal Care Committee. Six-week-old male spontaneously hyperlipidemic (SHL) mice (BALB/c. KOR/Stm Slc-Apoe$^{shl}$) with a disrupted apolipoprotein E (apoE) gene were purchased from Japan SLC (Shizuoka, Japan). These SHL mice were fed a diet high in fat and cholesterol (Western diet; containing 16.5% fat and 1.25% cholesterol; Western diet group) or a normal chow diet (normal diet group) for 14 weeks. Corresponding wild-type 6-week-old male BALB/cCrSlc mice (control group; Japan SLC, Shizuoka, Japan), as negative controls, were fed with a normal chow diet for 14 weeks. The 20-week-old mice were intravenously injected with IONP-ICG (55.8 mg Fe/kg, 1 mmol Fe/kg (33.2 nmol IONP-ICG/kg), 200 μl) via the tail vein. IONP-ICG5 and IONP-ICG10 were injected into mice in the Western diet group (n = 5), respectively, and IONP-ICG20 was injected into mice in the Western diet group (n = 5), normal diet group (n = 5), and control group (n = 5) (Supplemental Table 1).

### 2.5. Biodistribution study

To quantify the concentration of each type of IONP-ICG in the blood (percentage injected dose per gram of tissue (%ID/g)), mouse blood (2 μl) was collected at 5, 15, and 30 min and 1, 3, 6, 12, 24, and 48 h after each IONP-ICG injection. The half-life of the IONP-ICG in the blood was calculated using GraphPad Prism software (GraphPad Prism Software, La Jolla, CA). At 48 h after administration, mice were deeply anesthetized with an intraperitoneal injection of 50 mg/kg pentobarbital and perfused transcardially with 4% paraformaldehyde after 30 μl of blood was collected from the heart to measure the fluorescence intensity. Fluorescence images of tissues except the aorta were acquired using the IVIS Imaging System 200.

### 2.6. NIRF imaging and fluorescence quantitative analysis of arteriosclerotic plaque

The excised aorta was imaged ex vivo using a Nuance EX

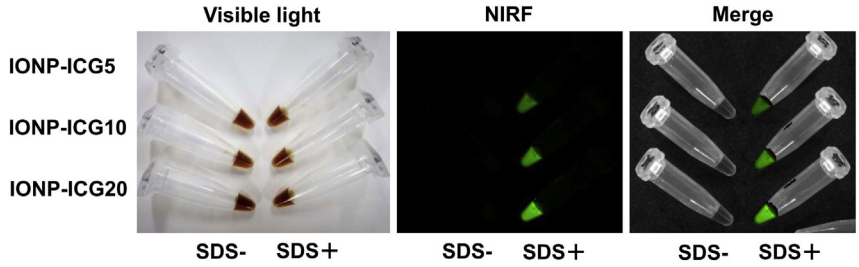


**Fig. 1.** Dequenching capacity of IONP-ICG probes.
Quenched (left) and chemically dequenched (right) IONP-ICG5, IONP-ICG10, and IONP-ICG20 are observed.

multispectral imaging camera (PerkinElmer) mounted on an Olympus MVX10 macro zoom fluorescence stereomicroscope (Olympus, Tokyo, Japan) equipped with a Cy7 filter set (excitation wavelength, 670–745 nm; emission filter, 776 nm long-pass). Visible-light and NIRF imaging were performed for both the ventral and dorsal sides.

### 2.7. Statistical analysis

Statistical analyses were performed using JMP version 11 software (SAS Institute, Cary, NC). Quantitative data were expressed as the mean ± standard deviation. Means were compared using two-way analysis of variance followed by the Tukey–Kramer test. Values of $p < 0.05$ were considered statistically significant.

## 3. Results

### 3.1. Characterization of IONP-ICG

The physicochemical properties of IONP-ICG are summarized in Supplemental Table 2. The numbers of ICG molecules conjugated with IONPs in IONP-ICG5, IONP-ICG10, and IONP-ICG20 were 3.1 ± 0.3, 6.1 ± 0.6, 9.2 ± 1.3, respectively (n = 6). As the reaction ratio of ICG to IONP increased, the number of ICG molecules bound to each IONP also increased. The hydrodynamic size of IONP-ICG5, IONP-ICG10, and IONP-ICG20 was 35.9 ± 8.2, 34.1 ± 10.1, and 34.9 ± 9.2 nm, respectively (n = 18). Compared with the parent nanoparticle (20-nm nanomag®-D-spio, 28.8 ± 6.9 nm; n = 18), the size of all probe nanoparticles increased because of the conjugated ICG-EG4-Sulfo-OSu and PEG-NHS ester molecules. The zeta potentials of IONP-ICG5, IONP-ICG10, and IONP-ICG20 were −0.3 ± 0.5, −0.4 ± 0.6, and −2.2 ± 1.1 mV, respectively (n = 18), and all probes showed negative charges compared with the parent nanoparticle (20-nm nanomag®-D-spio; 0.2 ± 0.4 mV; n = 18). NIRF intensity was low for all probes that were chemically quenched. By adding 1% sodium dodecyl sulfate (SDS) to the probes, intense NIRF was detected after denaturation. The dequenching capacity (fluorescence intensity of IONP-ICG incubated with 1% SDS in PBS/fluorescence intensity of IONP-ICG incubated in PBS) was 42 ± 4-fold, 44 ± 3-fold, and 60 ± 5-fold for IONP-ICG5, IONP-ICG10, and IONP-ICG20, respectively (Fig. 1; n = 3). As the conjugation ratio of ICG to IONP increased, the dequenching capacity improved. In NIRF analyses with SDS polyacrylamide gel electrophoresis (SDS-PAGE) (Supplemental Fig. 2), the noncovalent-binding fractions of ICG to IONP were analyzed. The chemical purities (number of ICG molecules covalently bound to IONP/total ICG molecules in IONP-ICG) for IONP-ICG5, IONP-ICG10, and IONP-ICG20 were 89% ± 3%, 93% ± 2%, and 88% ± 4% (n = 5).

### 3.2. Cellular uptake of IONP-ICG in macrophage cells

Microscopy studies (Fig. 2A) demonstrated that NIRF signals and the blue staining corresponding to iron oxide were not observed inside macrophages without IONP-ICG incubation. Slight NIRF and blue areas were visible inside macrophages after 1-h incubation. In bright-field imaging, brown areas corresponding to iron oxide were visible inside macrophages after 8-h incubation. As the incubation time and the number of ICG molecules conjugated with IONP increased, the NIRF signals observed in macrophages also increased. These results suggest that each IONP-ICG is activated after internalization to macrophage cells. In contrast, brown areas in the bright field and blue areas representing iron staining in macrophages showed no obvious change even when the number of ICG molecules conjugated with IONP increased. The uptake capacity of IONP-ICG by cultured human large vessel endothelial cells (Kurabo, Osaka, Japan) and human aortic smooth muscle cells (Promocell, Heidelberg, Germany) was extremely low compared to macrophages (Supplemental Fig. 3).

Cell pellets ($1 \times 10^6$ cells) with each IONP-ICG incubation were brown in visible light images, reflecting the uptake of IONP-ICG by macrophages, and the brown color became stronger as the incubation time was longer. Quantitative studies of NIRF intensity contained in macrophages showed that NIRF signals were observed in macrophages with IONP-ICG incubation for 1, 8, 24, and 48 h, and not observed without IONP-ICG incubation (Fig. 2B). As the incubation time and the number of ICG molecules conjugated with IONP increased, the NIRF signals observed in macrophages also significantly increased (Fig. 2C; n = 5). In contrast, iron contained in macrophages significantly increased with the incubation time, but there were no significant differences in iron contained in macrophages even when the number of ICG molecules conjugated with IONP increased (Fig. 2D; n = 5).

### 3.3. Biodistribution study

Accumulation of IONP-ICG in the blood was determined based on ICG fluorescence intensity (Supplemental Fig. 4A). All five groups showed similar concentrations of circulating IONP-ICG (%ID/g), which decreased over time, almost completely disappearing from the blood within 48 h. Circulation half-lives for IONP-ICG5, IONP-ICG10, IONP-ICG20 (Western diet group), IONP-ICG20 (normal diet group), and IONP-ICG20 (control group) were 197 ± 34, 164 ± 16, 174 ± 41, 183 ± 15, and 179 ± 33 min, respectively (Supplemental Fig. 4B). Significant differences in the circulating half-life of IONP-ICG were not observed between the five groups.

The results of biodistribution studies for IONP-ICG at 48 h after administration are summarized in Supplemental Table 3 and Supplemental Fig. 5). In each group, the greatest signal intensity was observed in the liver followed by the spleen. No significant

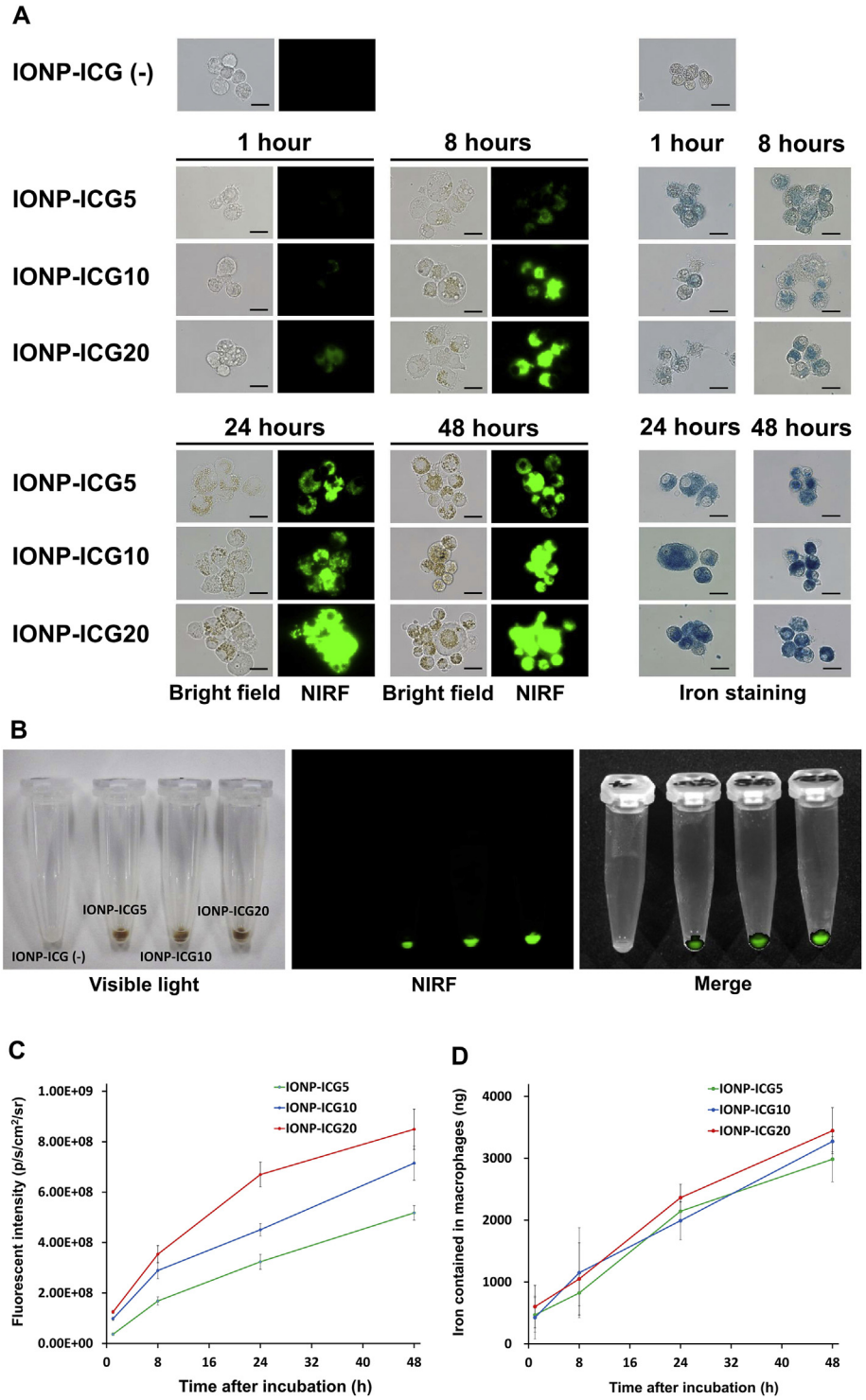


**Fig. 2.** Cellular uptake of IONP-ICG by macrophage cells.
(A) Macrophages were incubated with IONP-ICG5, IONP-ICG10, and IONP-ICG20 for 1, 8, 24, or 48 h. As the incubation time and the number of ICG molecules conjugated with IONPs increased, so did the intensity of the NIRF signals observed in the macrophages. In contrast, brown areas in the bright field and blue areas representing iron staining in macrophages showed no obvious change even when the number of ICG molecules conjugated with IONP increased. Scale bar indicates 20 μm. (B) Cell pellets ($1 \times 10^6$ cells) with each IONP-ICG incubation for 48 h were brown in visible light images, reflecting the uptake of IONP-ICG by macrophages. NIRF signals contained in macrophages were observed with each IONP-ICG incubation for 48 h and not observed without IONP-ICG incubation. (C) Quantitative studies of NIRF intensity contained in macrophages showed that as the incubation time and the number of ICG molecules conjugated with IONP increased, the NIRF signals observed in macrophages also significantly increased ($n = 5$). (D) Iron contained in macrophages significantly increased with the incubation time, but there were no significant differences in iron contained in macrophages even when the number of ICG molecules conjugated with IONP increased ($n = 5$).

differences between the five groups were seen for NIRF in the blood, which was designated as the surrounding tissue when atherosclerotic plaques were examined *in vivo*.

### 3.4. NIRF imaging and fluorescence quantitative analysis of arteriosclerotic plaque

Fig. 3A shows images of the aortas obtained from both the ventral and dorsal sides using fluorescence stereomicroscopy for SHL mice fed a Western diet and injected with IONP-ICG20. Visible-light imaging revealed white arteriosclerotic plaques in the aorta and the three branches. NIRF imaging showed clear and intense NIRF signals primarily at the margins of arteriosclerotic plaques, with relatively weak NIRF signals inside the plaques. As shown here, there is a localized NIRF intensity in the arteriosclerotic plaques, and detection of NIRF in the plaques was feasible.

The NIRF quantitative values per unit area ($n = 10$, signal count/$mm^2$) were measured at the aorta and the three branches from both the ventral and dorsal sides in each group of mice injected with IONP-ICG (Fig. 3D and E). In the Western diet groups, NIRF signals for IONP-ICG in the aorta regions increased linearly ($772{,}570 \pm 402{,}638$, $1{,}346{,}356 \pm 317{,}658$, and $2{,}400{,}773 \pm 657{,}044$ signals/$mm^2$ for IONP-ICG5, IONP-ICG10, and IONP-ICG20, respectively) as the number of ICG molecules attached to the IONPs increased (3.1, 6.1, and 9.2 for IONP-ICG5, IONP-ICG10, and IONP-ICG20, respectively; $R^2 = 0.9693$, Fig. 3F). In contrast, NIRF signals for IONP-ICG20 in the aorta and the three branches were significantly lower in the normal diet group ($1{,}028{,}516 \pm 365{,}834$ signals/$mm^2$) compared with the Western diet group ($2{,}400{,}773 \pm 657{,}044$ signals/$mm^2$). Mice in the control group did not display obvious white arteriosclerotic plaques in the aorta or the three branches under visible-light imaging, and the NIRF signal was similar to that in the blood vessels without arteriosclerotic plaques ($230{,}917 \pm 46{,}916$ signals/$mm^2$), which was significantly weaker in comparison with the Western and normal diet groups.

As mentioned above, higher NIRF signals were observed in the aortas of mice in the Western diet groups when the mice were intravenously injected with IONP-ICG loaded with many ICG molecules. However, independent of the number of ICGs conjugated to the IONPs, there was no significant difference in background signals in the blood, which can disrupt arteriosclerotic plaque imaging *in vivo*. Based on these results, IONP-ICG20 displayed the greatest lesion (arteriosclerotic plaque)-to-background (blood) ratio among the three types of probes and was considered the most effective probe for visualizing arteriosclerotic plaques. Thus, IONP-ICG20 was utilized for further imaging studies.

### 3.5. NIRF imaging with blood filled aorta

Since it was difficult to acquire images of mouse aorta *in vivo*, the aortas filled with blood were excised and observed using fluorescence microscopy to mimic *in vivo* conditions (Fig. 4). Visible-light imaging showed white arteriosclerotic plaques in the aorta and three branches. NIRF imaging detected clear and intense NIRF signals primarily at the margins of the arteriosclerotic plaques and relatively weak NIRF signals inside the plaques. High NIRF signals were observed especially at the arteriosclerotic plaques in the left common carotid arteries with low background signal from the blood.

### 3.6. Histological study and fluorescence microscopy study

Fig. 5 shows the histological findings for the aorta examined in Fig. 3A. Fluorescent microscopy of unstained slides showed localized NIRF signals at the intimal area of the arteriosclerotic plaque margin. Furthermore, the localization of NIRF signals in the arteriosclerotic plaques highly correlated with Iba-1-positive staining areas (localization of macrophages). In contrast, the localization of NIRF signals did not completely match with lipid accumulation in Oil Red O staining and most atherosclerotic plaques without NIRF signals also accumulated lipid. With iron staining, blue spots were observed for only a portion of the NIRF signal-positive intima regions. In particular, in arteriosclerotic plaques at the distal left subclavian arteries, which showed a particularly high intensity of iron staining (Fig. 5C), the co-localization of iron staining and ICG fluorescence signals was observed.

## 4. Discussion

In the present study, activatable NIRF IONP-ICG was synthesized and administered to SHL mice. We deduced that predominantly macrophages in atherosclerotic plaques phagocytosed this probe and activated NIRF in the probe inside the macrophages, though some NIRF signals might be influenced by endothelial cells and smooth muscle cells. In other words, it is thought that predominantly macrophage imaging using IONP-ICG in atherosclerotic plaques was feasible. The content and activity of macrophages in atherosclerotic plaques are related to the uptake of IONPs by macrophages [27,28]. Therefore, quantitative evaluation of NIRF signals in atherosclerotic plaques could not only determine the localization of macrophages but also act as an indicator of macrophage content or macrophage activation. Reducing dietary cholesterol intake facilitates the reduction of inflammation, improvement of endothelial cell dysfunction, and limitation of macrophage infiltration into the arteries [3,29–32]. In the present study, NIRF signals in the plaques were different for SHL mice injected with IONP-ICG20 and fed either a normal or Western diet, reflecting the number of macrophages present. Activatable fluorescence probes that emit fluorescence because of the action of inflammatory marker proteases, are also activated in an environment where extracellular proteases are present [5,21]. Since these proteases are secreted outside the cells and diffuse, the resulting fluorescence may not necessarily be retained at the inflammatory site. In contrast, the IONP-ICG probe used in the present study is thought to be a target cell-activatable probe internalized by target cells and activated intracellularly by lysosomal processing [33], leading to fluorescence activation within the target cells. Fluorescence is therefore localized within the target cells at the inflammatory site [17]. Because of this, it is thought that predominantly macrophage imaging using target cell-activatable probes was achieved with high background ratio.

Macrophage polarization creates mainly two different subsets, namely, M1 and M2 [2]. M1 macrophages are generally considered proinflammatory and thus facilitate the formation of the necrotic core and plaque destabilization. On the other hand, M2 macrophages are considered to have antiatherogenic properties, mediating plaque stability and are less susceptible to become foam cells [34]. Therefore, it is important to visualize the exact phenotypes of macrophages present in the atherosclerotic plaques for the prognosis, diagnosis, and treatment. However, since the uptake of IONPs by macrophages is independent of the macrophage differentiation into M1 or M2 cells *in vitro* [35], NIRF location in atherosclerotic plaques in the present study is considered to reflect the presence of macrophages, regardless of their specific subsets.

Pathophysiologically, circulating monocytes migrate from blood to the subendothelial space in response to signals and differentiate into inflammatory macrophages and foam cells during the formation of atherosclerotic plaques where macrophages locally proliferate [2,36], suggesting that most macrophages may accumulate at the luminal side of the intima. Migration and proliferation of

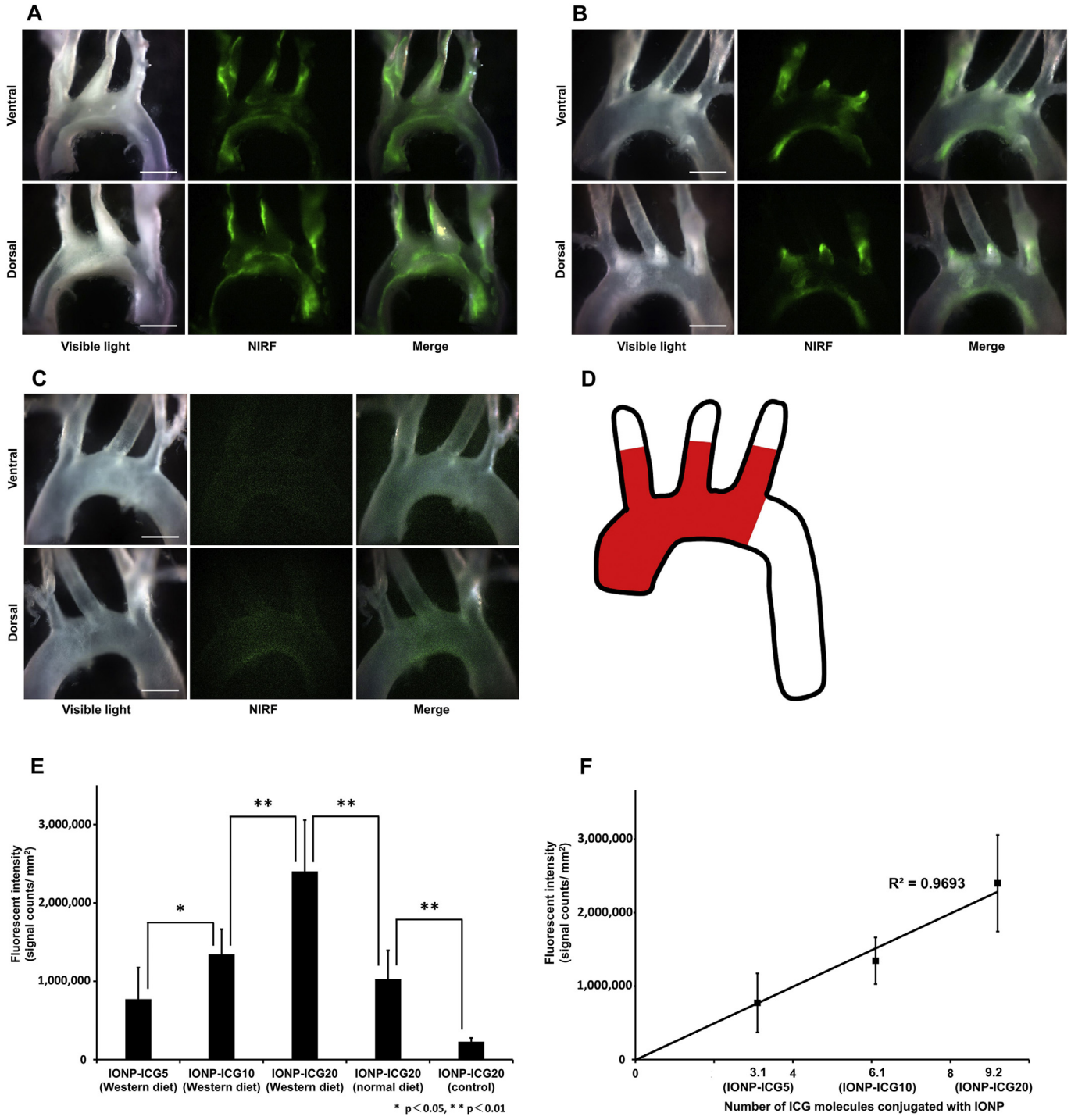


**Fig. 3.** NIRF imaging and fluorescence quantitative analysis of the aorta with or without atherosclerotic plaques.
(A–C) Visible-light and NIRF representative imaging of Western diet group (A), normal diet group (B), and control group (C) 48 h after intravenous administration of IONP-ICG20 were performed from both the ventral and dorsal sides of the aorta. IONP-ICG20 allows clear visualization of NIRF signals from atherosclerotic plaques. Scale bars indicate 1 mm. Original magnification ×25. (D) Schematic illustration presents the ROI as a red area drawn manually on the vessels including the ascending aorta, aortic arch (range from origin of the aorta to origin of the left subclavian artery), brachiocephalic artery, left common carotid artery, and left subclavian artery (range from origin of each artery to a distance of 1.0 mm from the origin). (E) Bar graph presents the quantitative NIRF value at the aorta with or without atherosclerotic plaques. IONP-ICG20 probe shows the highest NIRF intensity in aorta with atherosclerotic plaques. SHL mice with fewer arteriosclerotic plaques due to a normal diet showed a significantly lower NIRF signal intensity. Because wild-type mice in the control group showed no obvious arteriosclerotic plaques, NIRF signals were weak. All values are expressed as mean ± standard deviation (n = 10). (F) Mean fluorescent intensities are plotted relative to the number of ICG molecules conjugated with IONPs. NIRF intensity in the aorta with atherosclerotic plaques was linearly dependent on the number of ICG molecules conjugated with IONPs. Error bars represent the standard deviation.

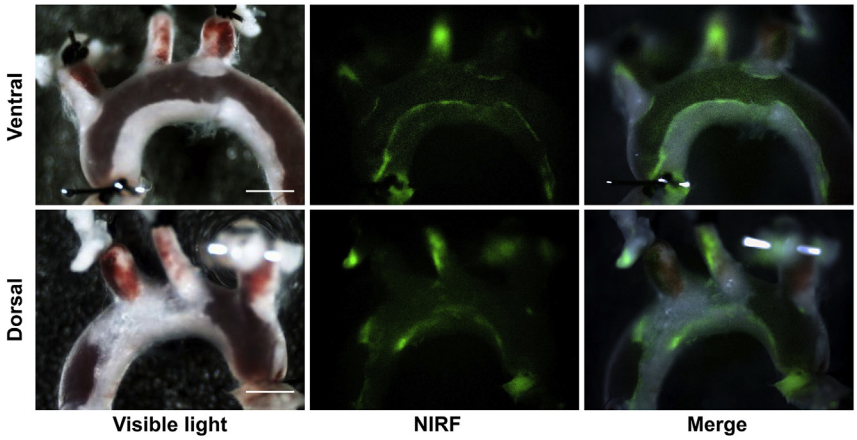


**Fig. 4.** NIRF image of the aorta filled with blood 48 h after intravenous administration of IONP-ICG20.
The NIRF signal in atherosclerotic plaques was detectable when the vessel and atherosclerotic plaques were exposed in the field of view. Scale bar indicates 1 mm. Original magnification ×25.

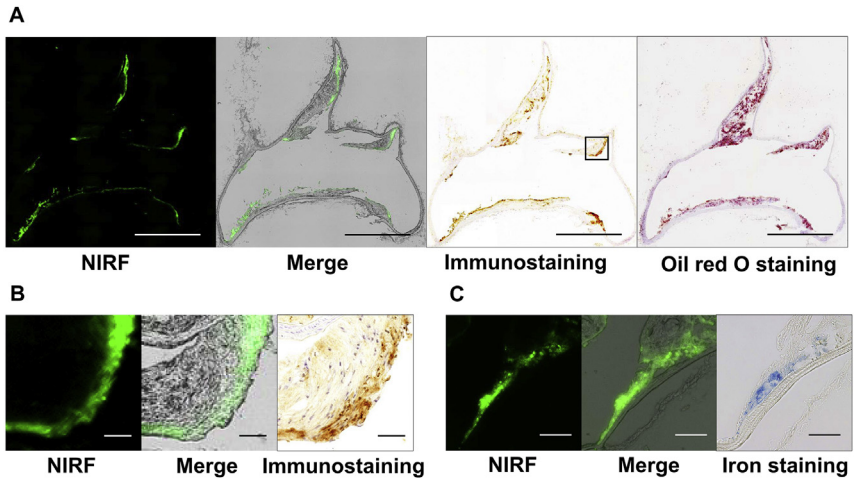


**Fig. 5.** Histology and fluorescence microscopy of the atherosclerotic plaques.
(A) NIRF, merged image of NIRF and bright-field imaging, Iba-1 immunostaining, and Oil Red O staining of the whole aorta with atherosclerotic plaques under low magnification. Scale bars indicate 1 mm. (B) NIRF, merger of NIRF and bright field, and Iba-1 immunostaining for the origin of the left subclavian artery, corresponding to the square area in Fig. 5A, are shown under high magnification. NIRF signals correlated very well with the presence of macrophage infiltration (Iba-1 immunostaining) in some atherosclerotic plaques, suggesting that NIRF signals were derived from the IONP-ICG probe phagocytized by macrophages. Scale bars indicate 50 μm. (C) NIRF, merging of NIRF and bright field, and iron staining of the distal portion of the left subclavian artery, in which blue spots are strongly stained, are shown under high magnification. Blue spots corresponding to iron oxide are observed within the area with NIRF signals. Scale bars indicate 50 μm.

vascular smooth muscle cells from the media toward the growing neointima also participate in plaque progression [37]. Since intimal proliferation spreads toward the luminal side like this, the accumulation of macrophages may remain at the luminal side of the plaques. Actually, many earlier studies using mouse models demonstrated accumulation of macrophages at the luminal side of plaques [5,20,21,36,38–43], and our present results are in line with these observations. From the findings of patterns of IONPs deposition in murine atherosclerosis and colocalization with macrophages, Klug et al. considered that IONPs passively diffuse via the luminal endothelium and are taken up by resident macrophages [44]. On the other hand, because of the fact that the localization of NIRF signals in the arteriosclerotic plaques is on the luminal side, IONP-ICG may tend to reach the luminal side of the plaques due to enhanced vascular permeability resulting from injured endothelium [27].

With regard to molecular imaging of atherosclerotic plaques, positron emission tomography (PET) using $^{18}$F-fluorodeoxyglucose ($^{18}$F-FDG) has been reported to be capable of detecting and quantifying atheroma inflammation by labeling macrophages *in vivo* and monitoring the treatment efficacy of anti-atherosclerosis therapy [45–48]. PET has high sensitivity, but this has limited spatial resolution and the additional disadvantage of requiring the use of radioactive agents. PET also lacks accuracy to assess the inflammation in a small artery in motion. Furthermore, it has been shown that $^{18}$F-FDG accumulates in vessel tissues without arteriosclerotic lesions induced by high fat diet, and thus careful evaluation is required for PET imaging [49]. Magnetic resonance imaging (MRI) with the use of IONPs has relatively high resolution, but low sensitivity and is difficult for quantitative analysis [24,25]. Contrast enhanced ultrasound has been reported to be capable of noninvasively imaging inflammatory response with microbubbles in atherosclerotic plaques [50,51]. This imaging modality is convenient, but limited spatial resolution. Compared to these noninvasive imaging modalities, NIRF imaging offers the potential for higher resolution and sensitivity and is applicable in real time

imaging, during invasive surgery and procedure. NIRF imaging is not competitive with the other non-invasive imaging modalities but is complementary. In addition, NIRF imaging is not widely used for the purpose of screening but for the purpose of providing support of surgery and procedure, suggesting that application of NIRF imaging for patients is limited to specific situations. Actually, it is necessary to surgically expose the vessel and atherosclerotic plaques in the field of view, or to use an intravascular NIRF imaging system in order to detect NIRF accumulating in atherosclerotic plaques *in vivo* [14,52]. Thus, NIRF imaging of atherosclerotic plaques cannot be achieved noninvasively. In addition, intravascular NIR imaging systems can't have spatial resolution like microscope used in our study.

Within the scope of this study, we could not detect significant changes in the circulating half-life of IONP-ICG even when the number of ICG molecules conjugated with the IONPs increased (Supplemental Fig. 4B), instead finding that the number of ICG molecules on each IONP was proportional to the NIRF signal in the atherosclerotic plaques (Fig. 3F). Based on these results, the probe can be considered to accumulate within the macrophages in atherosclerotic plaques without changing the circulatory dynamics, even with increases in the number of ICG molecules attached to each IONP. In general, when the number of biomolecules conjugated with the IONPs increases, the circulating half-life of the IONPs decreases, resulting in fewer IONPs reaching the target site [53]. This may occur because of increased hydrodynamic size when IONPs are conjugated with biomolecules [22]. The *in vivo* kinetics of carrier molecules are reportedly affected by an increase in the number of ICG molecules (molecular weight about 775 Da) conjugated with carrier molecules such as monoclonal antibodies (panitumumab; molecular weight about 147 kDa), human serum albumin (molecular weight, about 66 kDa), and water-soluble polymer (molecular weight, 25–50 kDa) [9,11,26]. The IONP (mean molecular weight, 3500 kDa) used in the present study has a larger molecular weight than the carrier molecules mentioned above. In other words, because individual IONPs have an extremely large molecular weight in comparison with ICG molecules, accumulation in the macrophages of atherosclerotic plaques might be possible without the latter significantly affecting the *in vivo* kinetics of the probe. Moreover, all three types of IONP-ICG had a hydrodynamic size of approximately 35 nm, resulting in similar circulating half-lives and ability to accumulate in macrophages within atherosclerotic plaques.

Circulating IONPs are primarily cleared by Kupffer cells in the liver and marginal zone macrophages, marginal zone metallophilic macrophages, and red pulp macrophages in spleen through the mononuclear phagocytic system or reticuloendothelial system [22,23]. In our biodistribution study, most NIRF signals were detected in the liver and spleen, demonstrating that these organs were indeed the primary metabolic sites for IONP-ICG. When excessive IONPs are administered, a portion of the circulating IONPs is taken up by macrophages in the liver and spleen, and the excess is taken up by other tissues such as the lungs and adipose tissue, where macrophages are abundant [54]. Since IONPs accumulate nonspecifically at macrophages in atherosclerotic plaques via this mechanism, the injection of a sufficient dose of IONPs is necessary for the accumulation of probes in macrophages within atherosclerotic plaques. The present study used an iron dose per body weight of 1 mmol Fe/kg (55.8 mg Fe/kg), a typical dose used in animal studies [42,55] that is at least 20 times greater than the clinical dose in humans (2.6 mg Fe/kg) [24,56]. Because rodents typically have a faster heart rate than humans, the circulating half-life of IONPs is markedly shorter [57]. Therefore, accumulation of IONPs at the atherosclerotic plaque macrophages in rodent models requires a higher dose of IONP compared with the dose used in clinical settings. Furthermore, the effects of blood vessel pulsation should be considered for actual evaluations *in vivo*.

Physicochemical properties such as hydrodynamic size, surface charge, and surface coating are considered factors that affect the *in vivo* biodistribution of IONPs [22]. Hydrodynamic size is considered to be one of the most crucial factors. At a size between 20 and 85 nm, the circulating half-life reportedly increases as the size decreases, facilitating macrophage accumulation of IONPs in organs other than the liver and spleen [22,58]. In contrast, hydrodynamic sizes of 0 to $\leq$10–15 nm lead to the excretion of IONP by the kidneys [59]. Uptake of the probe into atherosclerotic plaque macrophages is therefore postulated to be maximal for IONPs with a hydrodynamic size of approximately 20 nm. Because positively charged IONPs can interact with negatively charged plasma proteins, positively charged IONPs generally have a shorter half-life and are eliminated earlier from blood compared with negatively charged IONPs [60,61]. Since IONPs coated with numerous amino groups are predicted to be positively charged [62,63], we conjugated PEG to protect amino groups on the surface of IONPs after conjugation with ICG, resulting in a negatively charged final probe. Since uptake by Kupffer cells can be reduced through the stealth behavior of nanoparticle PEGylation, the circulating half-life of PEGylated IONPs is expected to increase [22].

In the present study, ICG fluorescent signals were localized in macrophage-rich regions; however, iron staining was mostly negative at the atherosclerotic plaques, where intense ICG fluorescent signals were observed. This is probably because the sensitivity for iron staining was insufficient due to relatively fewer infiltrating macrophages in the small plaque area. Moreover, iron staining might not be applicable for detecting IONPs prior to IONP degradation [54]. At 48-h after injection of the probe, the IONPs may not be stained sufficiently for degradation.

Macrophages play an important role in vascular inflammation and atherosclerosis [64,65], and contribute to coronary artery and cerebrovascular diseases. Anatomical factors such as plaque size and luminal stenosis do not necessarily correlate with macrophage content or activation. Macrophage imaging has been highlighted as a promising strategy to visualize clinically important unstable atherosclerotic plaques. Identifying the localization of unstable atherosclerotic plaques is crucial to prevent cerebral embolisms during carotid endarterectomy to treat internal carotid artery stenosis [66]. Macrophage imaging that would identify unstable atherosclerotic plaques may facilitate the process of deciding on the extent of atherosclerotic plaque resection and sites for arterial clamping in real time during carotid endarterectomy, providing support and assistance in surgeries. Furthermore, macrophage imaging of atherosclerotic plaques may not only identify the localization of inflamed plaques but also enable measurement of macrophage content or activation, indicating the potential for three-dimensional evaluation of the expression patterns of macrophages and for conducting further pathological analyses and clinical studies.

We describe that our study has some limitations. First, ApoE-knockout mice was an animal model absolutely accepted for atherosclerosis induction [67]. Among SHL mice, C57BL/6. KOR/Stm Slc-Apoe$^{shl}$, which are more akin to human pathology, develop the most severe atherosclerotic lesions [68]. Results from the present study using the BALB/c. KOR/Stm Slc-Apoe$^{shl}$ mice will have to be ascertained in a further study on ApoE knockout mice or C57BL/6. KOR/Stm Slc-Apoe$^{shl}$ mice in the future. Secondly, since animal model with atherosclerotic plaques cannot completely mimic human disease situation, careful extrapolation of our results to human disease should be made. Thirdly, Iba-1 is known to be expressed on activated endothelial and smooth muscle cells [69,70]. Therefore, the presence of these cells might contribute to Iba-1 positivity.

Some studies demonstrated that macrophages present in vascular lesions can be detected using Iba-1 [71–73]. Since the uptake capacity of IONP-ICG by endothelial cells and smooth muscle cells was extremely low compared to macrophages (Supplemental Fig. 3), macrophages seemed to be the predominant candidate for the uptake of IONP-ICG in atherosclerotic plaques. Furthermore, macrophages also take up IONPs to a greater extent than do endothelial and smooth muscle cells [27], supporting the view of higher uptake capacity of IONP-ICG by macrophages. Therefore, we believe that the regions for Iba-1 positivity and NIRF positivity are the areas of predominantly macrophage localization based on the results of *in vitro* experiments. However, since endothelial and smooth muscle cells in the inflammatory plaque environment may behave differently from unactivated cultured cells, we emphasize that some NIRF signals in the atherosclerotic plaques may come from these cells.

We demonstrated that macrophage imaging of atherosclerotic plaques could be feasible using activatable NIRF IONP-ICG. The number of ICG molecules conjugated with IONPs did not significantly affect the *in vivo* biodistribution; therefore, IONP-ICG20 showed the highest fluorescent signals for macrophages in atherosclerotic plaque regions. The materials used in this study (IONPs, ICG, and PEG) are highly biocompatible and are approved by the FDA [74]. Although studies confirming the safety of the final IONP-ICG conjugates synthesized with these reagents are necessary prior to use in humans, potential benefits in clinical translation are anticipated.

In conclusion, using activatable NIRF IONP-ICG, we would be able to identify the location of atherosclerotic plaque macrophages. Increasing the number of ICG molecules conjugated to IONPs led to increased NIRF signals in the macrophages surrounding atherosclerotic plaques as well as effective macrophage imaging. In contrast, reducing dietary cholesterol intake led to decreased NIRF signals in the atherosclerotic plaques. Quantitative evaluation of NIRF signals in atherosclerotic plaques may be an indicator of macrophage content or activation. The probe used in the present study was synthesized using highly biocompatible reagents, suggesting the potential for clinical applications in the future.

## Conflict of interest

The authors declared they do not have anything to disclose regarding conflict of interest with respect to this manuscript.

## Author contributions

H. I., A. I. and K.S. conceived and designed the study. H. I. and K. S. performed the experiments and wrote the paper. H. I. analyzed the data. All authors read, reviewed, edited and approved the manuscript.

## Acknowledgements

We are grateful to the laboratory staff in the Department of Patho-Functional Bioanalysis Graduate School of Pharmaceutical Sciences at Kyoto University for their valuable technical assistance. The authors would like to thank Enago (www.enago.jp) for the English language review.

## Appendix A. Supplementary data

Supplementary data related to this article can be found at https://doi.org/10.1016/j.atherosclerosis.2018.05.028.

## References

[1] M. Aikawa, P. Libby, Atherosclerotic plaque inflammation: the final frontier? Can. J. Cardiol. 20 (2004) 631–634.
[2] C.G. Santos-Gallego, B. Picatoste, J.J. Badimon, Pathophysiology of acute coronary syndrome, Curr. Atheroscler. Rep. 16 (2014) 401.
[3] M. Aikawa, E. Rabkin, S. Sugiyama, S.J. Voglic, Y. Fukumoto, Y. Furukawa, et al., An HMG-CoA reductase inhibitor, cerivastatin, suppresses growth of macrophages expressing matrix metalloproteinases and tissue factor *in vivo* and in vitro, Circulation 103 (2001) 276–283.
[4] D. Fukuda, E. Aikawa, F.K. Swirski, T.I. Novobrantseva, V. Kotelianski, C.Z. Gorgun, et al., Notch ligand delta-like 4 blockade attenuates atherosclerosis and metabolic disorders, Proc. Natl. Acad. Sci. U.S.A. 109 (2012) E1868–E1877.
[5] J.O. Deguchi, M. Aikawa, C.H. Tung, E. Aikawa, D.E. Kim, V. Ntziachristos, et al., Inflammation in atherosclerosis: visualizing matrix metalloproteinase action in macrophages in vivo, Circulation 114 (2006) 55–62.
[6] E. Aikawa, M. Nahrendorf, J.L. Figueiredo, F.K. Swirski, T. Shtatland, R.H. Kohler, et al., Osteogenesis associates with inflammation in early-stage atherosclerosis evaluated by molecular imaging in vivo, Circulation 116 (2007) 2841–2850.
[7] Y. Wang, J. Chen, B. Yang, H. Qiao, L. Gao, T. Su, et al., *In vivo* MR and fluorescence dual-modality imaging of atherosclerosis characteristics in mice using profilin-1 targeted magnetic nanoparticles, Theranostics 6 (2016) 272–286.
[8] G.R. Cherrick, S.W. Stein, C.M. Leevy, C.S. Davidson, Indocyanine green: observations on its physical properties, plasma decay, and hepatic extraction, J. Clin. Invest. 39 (1960) 592–600.
[9] K. Kanazaki, K. Sano, A. Makino, T. Homma, M. Ono, H. Saji, Polyoxazoline multivalently conjugated with indocyanine green for sensitive *in vivo* photoacoustic imaging of tumors, Sci. Rep. 6 (2016) 33798.
[10] K. Kanazaki, K. Sano, A. Makino, F. Yamauchi, A. Takahashi, T. Homma, et al., Feasibility of poly(ethylene glycol) derivatives as diagnostic drug carriers for tumor imaging, J. Control. Release. 226 (2016) 115–123.
[11] K. Kanazaki, K. Sano, A. Makino, A. Takahashi, J. Deguchi, M. Ohashi, et al., Development of human serum albumin conjugated with near-infrared dye for photoacoustic tumor imaging, J. Biomed. Optic. 19 (2014) 96002.
[12] K. Sano, T. Nakajima, K. Miyazaki, Y. Ohuchi, T. Ikegami, P.L. Choyke, et al., Short PEG-linkers improve the performance of targeted, activatable monoclonal antibody-indocyanine green optical imaging probes, Bioconjugate Chem. 24 (2013) 811–816.
[13] M. Ogawa, N. Kosaka, P.L. Choyke, H. Kobayashi, *In vivo* molecular imaging of cancer with a quenching near-infrared fluorescent probe using conjugates of monoclonal antibodies and indocyanine green, Canc. Res. 69 (2009) 1268–1272.
[14] C. Vinegoni, I. Botnaru, E. Aikawa, M.A. Calfon, Y. Iwamoto, E.J. Folco, et al., Indocyanine green enables near-infrared fluorescence imaging of lipid-rich, inflamed atherosclerotic plaques, Sci. Transl. Med. 3 (2011) 84ra45.
[15] J.W. Verjans, E.A. Osborn, G.J. Ughi, M.A. Calfon Press, E. Hamidi, A.P. Antoniadis, et al., Targeted near-infrared fluorescence imaging of atherosclerosis: clinical and intracoronary evaluation of indocyanine green, JACC Cardiovasc Imaging. 9 (2016) 1087–1095.
[16] T. Desmettre, J.M. Devoisselle, S. Mordon, Fluorescence properties and metabolic features of indocyanine green (ICG) as related to angiography, Surv. Ophthalmol. 45 (2000) 15–27.
[17] Y. Hama, Y. Urano, Y. Koyama, M. Kamiya, M. Bernardo, R.S. Paik, et al., A target cell-specific activatable fluorescence probe for *in vivo* molecular imaging of cancer based on a self-quenched avidin-rhodamine conjugate, Canc. Res. 67 (2007) 2791–2799.
[18] Y. Urano, D. Asanuma, Y. Hama, Y. Koyama, T. Barrett, M. Kamiya, et al., Selective molecular imaging of viable cancer cells with pH-activatable fluorescence probes, Nat. Med. 15 (2009) 104–109.
[19] M. Ogawa, C.A. Regino, P.L. Choyke, H. Kobayashi, *In vivo* target-specific activatable near-infrared optical labeling of humanized monoclonal antibodies, Mol. Canc. Therapeut. 8 (2009) 232–239.
[20] J.B. Kim, K. Park, J. Ryu, J.J. Lee, M.W. Lee, H.S. Cho, et al., Intravascular optical imaging of high-risk plaques *in vivo* by targeting macrophage mannose receptors, Sci. Rep. 6 (2016) 22608.
[21] D.E. Kim, J.Y. Kim, D. Schellingerhout, S.M. Shon, S.W. Jeong, E.J. Kim, et al., Molecular imaging of cathepsin B proteolytic enzyme activity reflects the inflammatory component of atherosclerotic pathology and can quantitatively demonstrate the antiatherosclerotic therapeutic effects of atorvastatin and glucosamine, Mol. Imag. 8 (2009) 291–301.
[22] H. Arami, A. Khandhar, D. Liggitt, K.M. Krishnan, *In vivo* delivery, pharmacokinetics, biodistribution and toxicity of iron oxide nanoparticles, Chem. Soc. Rev. 44 (2015) 8576–8607.
[23] Y.X. Wang, S.M. Hussain, G.P. Krestin, Superparamagnetic iron oxide contrast agents: physicochemical characteristics and applications in MR imaging, Eur. Radiol. 11 (2001) 2319–2331.
[24] M.E. Kooi, V.C. Cappendijk, K.B. Cleutjens, A.G. Kessels, P.J. Kitslaar, M. Borgers, et al., Accumulation of ultrasmall superparamagnetic particles of iron oxide in human atherosclerotic plaques can be detected by *in vivo* magnetic resonance imaging, Circulation 107 (2003) 2453–2458.
[25] S.G. Ruehm, C. Corot, P. Vogt, S. Kolb, J.F. Debatin, Magnetic resonance imaging

of atherosclerotic plaque with ultrasmall superparamagnetic particles of iron oxide in hyperlipidemic rabbits, Circulation 103 (2001) 415–422.
[26] K. Sano, M. Ohashi, K. Kanazaki, N. Ding, J. Deguchi, Y. Kanada, et al., *In vivo* photoacoustic imaging of cancer using indocyanine green-labeled monoclonal antibody targeting the epidermal growth factor receptor, Biochem Biophys Res Commum. 464 (2015) 820–825.
[27] K. Morishige, D.F. Kacher, P. Libby, L. Josephson, P. Ganz, R. Weissleder, et al., High-resolution magnetic resonance imaging enhanced with superparamagnetic nanoparticles measures macrophage burden in atherosclerosis, Circulation 122 (2010) 1707–1715.
[28] C. von Zur Muhlen, D. von Elverfeldt, N. Bassler, I. Neudorfer, B. Steitz, A. Petri-Fink, et al., Superparamagnetic iron oxide binding and uptake as imaged by magnetic resonance is mediated by the integrin receptor Mac-1 (CD11b/CD18): implications on imaging of atherosclerotic plaques, Atherosclerosis 193 (2007) 102–111.
[29] M. Aikawa, P. Libby, The vulnerable atherosclerotic plaque: pathogenesis and therapeutic approach, Cardiovasc. Pathol. 13 (2004) 125–138.
[30] P. Libby, M. Aikawa, Stabilization of atherosclerotic plaques: new mechanisms and clinical targets, Nat. Med. 8 (2002) 1257–1262.
[31] M. Aikawa, E. Rabkin, Y. Okada, S.J. Voglic, S.K. Clinton, C.E. Brinckerhoff, et al., Lipid lowering by diet reduces matrix metalloproteinase activity and increases collagen content of rabbit atheroma: a potential mechanism of lesion stabilization, Circulation 97 (1998) 2433–2444.
[32] M. Aikawa, S. Sugiyama, C.C. Hill, S.J. Voglic, E. Rabkin, Y. Fukumoto, et al., Lipid lowering reduces oxidative stress and endothelial cell activation in rabbit atheroma, Circulation 106 (2002) 1390–1396.
[33] K. Muller, J.N. Skepper, M. Posfai, R. Trivedi, S. Howarth, C. Corot, et al., Effect of ultrasmall superparamagnetic iron oxide nanoparticles (Ferumoxtran-10) on human monocyte-macrophages in vitro, Biomaterials 28 (2007) 1629–1642.
[34] G. Chinetti-Gbaguidi, M. Baron, M.A. Bouhlel, J. Vanhoutte, C. Copin, Y. Sebti, et al., Human atherosclerotic plaque alternative macrophages display low cholesterol handling but high phagocytosis because of distinct activities of the PPARγ and LXRα pathways, Circ. Res. 108 (2011) 985–995.
[35] T. Aoki, M. Saito, H. Koseki, K. Tsuji, A. Tsuji, K. Murata, et al., Macrophage imaging of cerebral aneurysms with ferumoxytol: an exploratory study in an animal model and in patients, J. Stroke Cerebrovasc. Dis. 26 (2017) 2055–2064.
[36] C.S. Robbins, I. Hilgendorf, G.F. Weber, I. Theurl, Y. Iwamoto, J.L. Figueiredo, et al., Local proliferation dominates lesional macrophage accumulation in atherosclerosis, Nat. Med. 19 (2013) 1166–1172.
[37] P. Lacolley, V. Regnault, A. Nicoletti, Z. Li, J.B. Michel, The vascular smooth muscle cell in arterial pathology: a cell that can take on multiple roles, Cardiovasc. Res. 95 (2012) 194–204.
[38] J.B. Morris, A.R. Olzinski, R.E. Bernard, K. Aravindhan, R.C. Mirabile, R. Boyce, et al., p38 MARK inhibition reduces aortic ultrasmall superparamagnetic iron oxide uptake in a mouse model of atherosclerosis: MRI assessment, Arterioscler. Thromb. Vasc. Biol. 28 (2008) 265–271.
[39] G. Klug, T. Kampf, C. Ziener, M. Parczyk, E. Bauer, V. Herold, et al., Murine atherosclerotic plaque imaging with the USPIO Ferumoxtran-10, Front. Biosci. 14 (2009) 2546–2552.
[40] M. Matsumoto, M. Sata, D. Fukuda, K. Tanaka, M. Soma, Y. Hirata, et al., Orally administered eicosapentaenoic acid reduces and stabilizes atherosclerotic lesions in ApoE-deficient mice, Atherosclerosis 197 (2008) 524–533.
[41] K. Yamamoto, H. Miyoshi, K.Y. Cho, A. Nakamura, A.S. Greenberg, T. Atsumi, Overexpression of perilipin1 protects against atheroma progression in apolipoprotein E knockout mice, Atherosclerosis 269 (2018) 192–196.
[42] M. Sigovan, A. Bessaad, H. Alsaid, E. Lancelot, C. Corot, B. Neyran, et al., Assessment of age modulated vascular inflammation in ApoE-/- mice by USPIO-enhanced magnetic resonance imaging, Invest. Radiol. 45 (2010) 702–707.
[43] A. Diez-Juan, P. Perez, M. Aracil, D. Sancho, A. Bernad, F. Sanchez-Madrid, et al., Selective inactivation of p27(Kip1) in hematopoietic progenitor cells increases neointimal macrophage proliferation and accelerates atherosclerosis, Blood 103 (2004) 158–161.
[44] G. Klug, L. Bauer, W.R. Bauer, Patterns of USPIO deposition in murine atherosclerosis, Arterioscler. Thromb. Vasc. Biol. 28 (2008). E157.
[45] J.M. Tarkin, F.R. Joshi, J.H. Rudd, PET imaging of inflammation in atherosclerosis, Nat. Rev. Cardiol. 11 (2014) 443–457.
[46] E.J. Folco, Y. Sheikine, V.Z. Rocha, T. Christen, E. Shvartz, G.K. Sukhova, et al., Hypoxia but not inflammation augments glucose uptake in human macrophages: implications for imaging atherosclerosis with 18fluorine-labeled 2-deoxy-D-glucose positron emission tomography, J. Am. Coll. Cardiol. 58 (2011) 603–614.
[47] J.H. Rudd, E.A. Warburton, T.D. Fryer, H.A. Jones, J.C. Clark, N. Antoun, et al., Imaging atherosclerotic plaque inflammation with [18F]-fluorodeoxyglucose positron emission tomography, Circulation 105 (2002) 2708–2711.
[48] N. Tahara, H. Kai, M. Ishibashi, H. Nakaura, H. Kaida, K. Baba, et al., Simvastatin attenuates plaque inflammation: evaluation by fluorodeoxyglucose positron emission tomography, J. Am. Coll. Cardiol. 48 (2006) 1825–1831.
[49] Y. Zhao, Y. Kuge, S. Zhao, H.W. Strauss, F.G. Blankenberg, N. Tamaki, Prolonged high-fat feeding enhances aortic 18f-FDG and 99mTc-annexin A5 uptake in apolipoprotein E-deficient and wild-type C57BL/6J mice, J. Nucl. Med. 49 (2008) 1707–1714.
[50] R. Sun, J. Tian, J. Zhang, L. Wang, J. Guo, Y. Liu, Monitoring inflammation injuries in the progression of atherosclerosis with contrast enhanced ultrasound molecular imaging, PLoS One 12 (2017) e0186155.
[51] X. Li, R. Zhang, Z. Li, C. Ning, Z. Wang, M. Dang, et al., Contrast-enhanced ultrasound imaging quantification of adventitial vasa vasorum in a rabbit model of varying degrees of atherosclerosis, Sci. Rep. 7 (2017) 7032.
[52] F.A. Jaffer, C. Vinegoni, M.C. John, E. Aikawa, H.K. Gold, A.V. Finn, et al., Real-time catheter molecular sensing of inflammation in proteolytically active atherosclerosis, Circulation 118 (2008) 1802–1809.
[53] J.H. Park, G. von Maltzahn, L. Zhang, A.M. Derfus, D. Simberg, T.J. Harris, et al., Systematic surface engineering of magnetic nanoworms for *in vivo* tumor targeting, Small 5 (2009) 694–700.
[54] M. Levy, N. Luciani, D. Alloyeau, D. Elgrabli, V. Deveaux, C. Pechoux, et al., Long term *in vivo* biotransformation of iron oxide nanoparticles, Biomaterials 32 (2011) 3988–3999.
[55] M. Sigovan, L. Boussel, A. Sulaiman, D. Sappey-Marinier, H. Alsaid, C. Desbleds-Mansard, et al., Rapid-clearance iron nanoparticles for inflammation imaging of atherosclerotic plaque: initial experience in animal model, Radiology 252 (2009) 401–409.
[56] R.A. Trivedi, J.M. UK-I, M.J. Graves, J.J. Cross, J. Horsley, M.J. Goddard, et al., *In vivo* detection of macrophages in human carotid atheroma: temporal dependence of ultrasmall superparamagnetic particles of iron oxide-enhanced MRI, Stroke 35 (2004) 1631–1635.
[57] Z. Lin, N.A. Monteiro-Riviere, J.E. Riviere, Pharmacokinetics of metallic nanoparticles, Wiley Interdiscip Rev Nanomed Nanobiotechnol. 7 (2015) 189–217.
[58] F. Roohi, J. Lohrke, A. Ide, G. Schutz, K. Dassler, Studying the effect of particle size and coating type on the blood kinetics of superparamagnetic iron oxide nanoparticles, Int. J. Nanomed. 7 (2012) 4447–4458.
[59] M. Longmire, P.L. Choyke, H. Kobayashi, Clearance properties of nano-sized particles and molecules as imaging agents: considerations and caveats, Nanomedicine 3 (2008) 703–717.
[60] B. Chertok, A.E. David, V.C. Yang, Polyethyleneimine-modified iron oxide nanoparticles for brain tumor drug delivery using magnetic targeting and intra-carotid administration, Biomaterials 31 (2010) 6317–6324.
[61] U. Sakulkhu, M. Mahmoudi, L. Maurizi, J. Salaklang, H. Hofmann, Protein corona composition of superparamagnetic iron oxide nanoparticles with various physico-chemical properties and coatings, Sci. Rep. 4 (2014) 5020.
[62] A.J. Cole, A.E. David, J. Wang, C.J. Galban, H.L. Hill, V.C. Yang, Polyethylene glycol modified, cross-linked starch-coated iron oxide nanoparticles for enhanced magnetic tumor targeting, Biomaterials 32 (2011) 2183–2193.
[63] M. Mahmoudi, S. Sheibani, A.S. Milani, F. Rezaee, M. Gauberti, R. Dinarvand, et al., Crucial role of the protein corona for the specific targeting of nanoparticles, Nanomedicine 10 (2015) 215–226.
[64] I. Tabas, K.E. Bornfeldt, Macrophage phenotype and function in different stages of atherosclerosis, Circ. Res. 118 (2016) 653–667.
[65] I. Tabas, 2016 russell ross memorial lecture in vascular biology: molecular-cellular mechanisms in the progression of atherosclerosis, Arterioscler. Thromb. Vasc. Biol. 37 (2017) 183–189.
[66] N. Altaf, A. Beech, S.D. Goode, J.R. Gladman, A.R. Moody, D.P. Auer, et al., Carotid intraplaque hemorrhage detected by magnetic resonance imaging predicts embolization during carotid endarterectomy, J. Vasc. Surg. 46 (2007) 31–36.
[67] C.G. Santos-Gallego, J.J. Badimon, B. Ibáñez, Modelos experimentales de aterosclerosis, Rev Esp Cardiol Supl 13 (E) (2013) 3–12.
[68] Y. Matsushima, T. Sakurai, A. Ohoka, T. Ohnuki, N. Tada, Y. Asoh, et al., Four strains of spontaneously hyperlipidemic (SHL) mice: phenotypic distinctions determined by genetic backgrounds, J Athrroscler Thromb. 8 (2001) 71–79.
[69] M.V. Autieri, C. Carbone, A. Mu, Expression of allograft inflammatory factor-1 is a marker of activated human vascular smooth muscle cells and arterial injury, Arterioscler. Thromb. Vasc. Biol. 20 (2000) 1737–1744.
[70] Y. Tian, S. Jain, S.E. Kelemen, M.V. Autieri, AIF-1 expression regulates endothelial cell activation, signal transduction, and vasculogenesis, Am. J. Physiol. Cell Physiol. 296 (2009) C256–C266.
[71] T. Mishima, K. Iwabuchi, S. Fujii, S.Y. Tanaka, H. Ogura, K. Watano-Miyata, et al., Allograft inflammatory factor-1 augments macrophage phagocytotic activity and accelerates the progression of atherosclerosis in ApoE-/- mice, Int Mol Med. 21 (2008) 181–187.
[72] T. Ikedo, M. Minami, H. Kataoka, K. Hayashi, M. Nagata, R. Fujikawa, et al., Dipeptidyl peptidase-4 inhibitor anagliptin prevents intracranial aneurysm growth by suppressing macrophage infiltration and activation, J Am Heart Assoc. 6 (2017) e004777.
[73] Y. Tian, S.E. Kelemen, M.V. Autieri, Inhibition of AIF-1 expression by constitutive siRNA expression reduces macrophage migration, proliferation, and signal transduction initiated by atherogenic stimuli, Am. J. Physiol. Cell Physiol. 290 (2006) C1083–C1091.
[74] C. Fruijtier-Polloth, Safety assessment on polyethylene glycols (PEGs) and their derivatives as used in cosmetic products, Toxicology 214 (2005) 1–38.